



ELSEVIER

Available online at www.sciencedirect.com

SCIENCE @ DIRECT®

Geotextiles and Geomembranes 21 (2003) 151–175

www.elsevier.com/locate/geotextmem

Geotextiles
and
Geomembranes

Geosynthetic reinforced embankments on soft clay foundations: predicting reinforcement strains at failure[☆]

Sean D. Hinchberger^a, R. Kerry Rowe^{b,*}

^a *Acres International Limited, 4342 Queen Street, P.O. Box 1001, Niagara Falls, Ont., Canada L2E 6W1*

^b *Department of Civil Engineering, Queen's University, 99 University Avenue, Kingston, Ont., Canada K7L 3N6*

Received 14 November 2002; received in revised form 23 December 2002; accepted 3 January 2003

Abstract

Geosynthetic reinforced embankments can fail before the ultimate tensile strength of the reinforcement is mobilized. For the purpose of embankment design, engineers must often rely on experience when selecting a reinforcement strain for analysis using limit equilibrium methods or resort to complicated numerical methods such as those based on the finite element method. This paper presents a simple procedure for estimating the undrained stability of geosynthetic reinforced embankments founded on soft clayey soils where the shear strength increases with depth. Finite element results are summarized in a design chart for establishing geosynthetic reinforcement strains suitable for design. The procedure is illustrated using worked examples and tested against a well documented case history.

© 2003 Elsevier Science Ltd. All rights reserved.

Keywords: Embankment; Geosynthetic; Reinforcement; Design; Limit equilibrium; Finite element analysis; Soft clay

1. Introduction

Limit equilibrium techniques have become accepted as a method of assessing the undrained stability of reinforced embankments founded on soft clayey soils (Jewel, 1982; Milligan and La Rochelle, 1984; Rowe and Soderman, 1985; Bergado et al.,

[☆]Prof. S.A. Tan acted as editor for the review of this paper.

*Corresponding author. Tel.: +1-613-533-6933; fax: +1-613-533-6934.

E-mail addresses: shinchberger@acres.com (S.D. Hinchberger), kerry@civil.queensu.ca (R.K. Rowe).

Nomenclature

c_{u0}	undrained shear strength at the foundation surface
E_u	undrained Young's modulus
ρ_c	increase of undrained shear strength with depth
D	depth of soft clay deposit
n	embankment side slope gradient ($nH:1V$)
h	design embankment height
B	embankment crest width
PF	partial factor
c_{u0}^*, ρ_c^*	factored shear strength parameters
H_c	collapse height of an unreinforced embankment
H_u	collapse height of a perfectly reinforced embankment
H_f	calculated embankment fill thickness at failure
T_a	allowable reinforcement force
T_r	reinforcement force required for stability
m	number of reinforcement layers
J	reinforcement secant stiffness
J_{crit}	critical reinforcement secant stiffness
J_{FE}	reinforcement stiffness in finite element calculations
J_{LE}	reinforcement stiffness in limit equilibrium calculations
ϵ_r	reinforcement strain
ϵ_a	allowable reinforcement strain ($\epsilon_a \approx \epsilon_0$ for $J \leq J_{crit}$)
ϵ_0	critical reinforcement strain for $J < J_{crit}$
ϵ_p	performance limit strain of reinforcement
E	Young's modulus
P_a	atmospheric pressure
σ_3	minor principle stress
K_E, M	material constants for Janbu's equation
ϕ'	internal angle of friction
γ_{fill}	bulk unit weight of fill
K'_0	coefficient of lateral earth pressure at rest
α_r	reinforcement correction factor
φ	dilatancy angle
ν	Poisson's ratio
γ_{bulk}	Bulk unit weight of fill

1994; Palmeira et al., 1998, etc.). The application of this approach, however, assumes that the reinforcement strain at failure is known (Rowe and Soderman, 1985, 1987). For the purpose of embankment design, engineers are often required to rely on either experience or complicated methods of analysis (e.g. finite element methods) to estimate reinforcement strains for use in limit equilibrium calculations

(e.g. Bonaparte and Christopher, 1987). Utilizing the ultimate tensile strain of geosynthetic reinforcement in design calculations (e.g. Michalowski, 1992) can lead to overestimation of the factor of safety since reinforced embankments may fail due to excessive displacements before failure of the reinforcement (Rowe and Soderman, 1987; Rowe et al., 1995).

Rowe and Soderman (1985) introduced a method for estimating the allowable reinforcement strain at failure for use with slip circle analysis. The method is limited to embankments constructed on clayey soils with an approximately uniform strength with depth. To date, few guidelines exist for estimating the allowable reinforcement strains at failure for embankments founded on clayey soils where the undrained shear strength increases with depth (Rowe and Mylleville, 1989).

This paper presents an approximate method for estimating geosynthetic reinforcement strains at failure and the resultant undrained stability of reinforced embankments constructed on soft clayey foundation soils. The foundation soils are assumed to have increasing undrained shear strength with depth. A well documented case history is used to test the method which is illustrated by two worked examples.

2. Design approach

Fig. 1 shows the geometry of a typical embankment fill with height, h , crest width, B , and side slope $nH:1V$ constructed on a soft clay foundation of depth D . The undrained shear strength of the foundation soil is represented by the undrained shear strength at the foundation surface, c_{u0} , and the increase of undrained shear strength

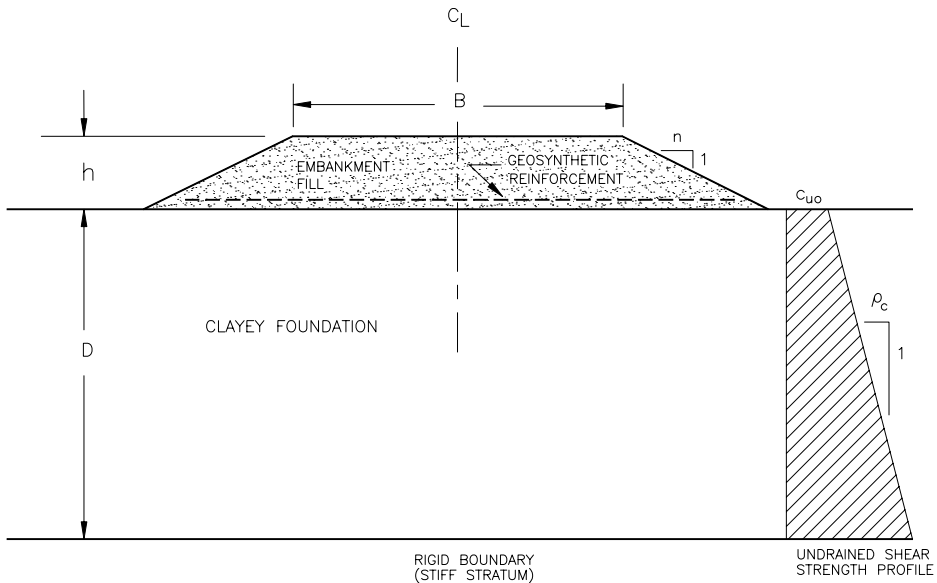


Fig. 1. Generalized embankment geometry and foundation soil stratigraphy.

with depth, ρ_c . For the design of embankments founded on soft clayey soils, the designer may choose to use geosynthetic reinforcement to ensure adequate end-of-construction or undrained stability. Below, a simplified design process for estimating the degree of reinforcement necessary to achieve adequate embankment stability is described.

2.1. Factored soil strength parameters

Assuming the undrained shear strength of the foundation soil has been adequately defined, the first step in design is to obtain factored soil parameters (c_{u0}^* and ρ_c^*) by applying an appropriate partial factor, PF . In this paper, a partial factor of $PF = (1/1.3) = 0.77$ will be adopted yielding factored strength properties $c_{u0}^* = PF \times c_{u0}$ and $\rho_c^* = PF \times \rho_c$. For an unreinforced embankment, adopting a partial factor, $PF = 0.77$, is equivalent to adopting a factor of safety of 1.3 against failure of the foundation soil.

2.2. Collapse height of an unreinforced embankment

Next, a conventional limit equilibrium (slip circle) analysis must be performed using factored soil properties to assess if reinforcement is required. If the calculated collapse height of an unreinforced embankment, H_c , is equal to or greater than the required embankment height, the design is complete and reinforcement is not required. Otherwise, reinforcement may be considered to allow additional fill height. In the context of limit state design, the collapse height H_c of the unreinforced embankment corresponds to the height at which the overturning moment is equal to the restoring moment when factored soil parameters are used.

2.3. Collapse height of a perfectly reinforced embankment

If reinforcement is considered to achieve the required design embankment height, the next step in the design is to calculate the theoretical maximum height, H_u , of a perfectly reinforced embankment as described by [Rowe and Soderman \(1987\)](#), [Rowe and Mylleville \(1993\)](#) and [Leroueil and Rowe \(2001\)](#). Again factored soil strength parameters are adopted and here it is assumed that there is sufficient reinforcement to cause the embankment to behave as a rigid footing. The collapse height, H_u , is calculated using bearing capacity solutions for rigid footings adapted for the analysis of embankment loading and geometry.

If the required design height, h , exceeds the maximum height of a perfectly reinforced embankment (i.e. $h > H_u$) then reinforcement alone will not provide adequate stability and alternative means of stabilization (e.g. use of light weight fill, prefabricated vertical drains, or stage construction) will be required. If the design height, h , exceeds H_c but is less than H_u , then it is necessary to select reinforcement that will provide the required stabilizing force.

2.4. Reinforcement forces for reinforced embankment stability

The stability of a proposed reinforcement scheme can be assessed by performing limit equilibrium analysis (e.g. Rowe and Soderman, 1985; Rowe and Mylleville, 1993; Palmeira et al., 1998) where there is an additional restoring moment due to the force T mobilized by the inclusion of reinforcement. The reinforcement force, T , can be taken as the minimum of:

- (i) the force required to support the outward shear stresses at the clay-fill interface beneath the embankment and the thrust force in the embankment fill (Jewel, 1988);
- (ii) the pullout capacity of the reinforcement (e.g. Fowler and Koerner, 1987);
- (iii) the allowable force.

$$T_a = mJ\varepsilon_a,$$

where m is the number of layers of reinforcement and m is small (typically $m = 1-2$; see Rowe and Mylleville, 1990); J the reinforcement secant stiffness over the strain range 0 to ε_a ; ε_a the allowable reinforcement strain.

Selection of the allowable reinforcement strain for use in design is not a trivial exercise. An upper bound for ε_a is the performance limit strain, ε_p , of the reinforcement under consideration (e.g. see McGown et al., 1995; den Hoedt, 1986). Adopting $\varepsilon_a = \varepsilon_p$ for design, however, may produce a marginal design since reinforced embankments can fail due to excessive displacement before the performance limit strain of the reinforcement is reached. The design curves shown in Fig. 2 have been developed for estimating the allowable reinforcement strain, ε_a ,

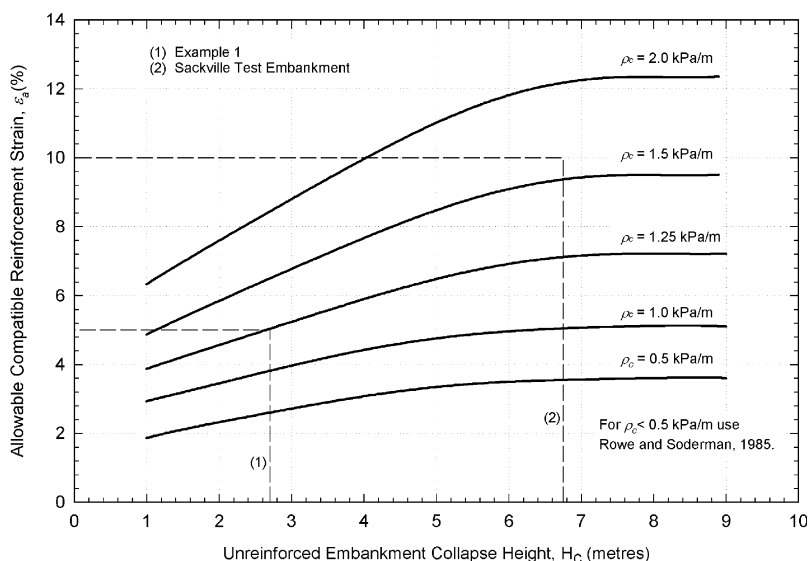


Fig. 2. Design chart.

for the case where embankment failure occurs due to excessive displacement. The method is applicable to soils where the strength increases with depth. In design, the allowable reinforcement strain will be the minimum of that deduced from Fig. 2 and the performance limit strain.

The remainder of this paper will focus on the basis for the development of Fig. 2 and estimation of the allowable compatible strain for embankments built on soft clayey foundations where the strength increases with depth.

3. Numerical methods

The finite element method has been used by many researchers to investigate the behaviour of reinforced embankments (e.g. Rowe, 1982, 1984; Rowe and Soderman, 1984; Humphrey and Holtz, 1989; Hird and Kwok, 1989; Rowe and Myleville, 1990; Bergado et al., 2002). Details regarding the finite element procedure, choice of elements and constitutive modelling adopted in the present study are the same as previously described by Rowe and Soderman (1987) and elaborated on by Rowe and Myleville (1993) and Leroueil and Rowe (2001).

The embankment fill was modelled as a frictional material with a friction angle $\phi' = 32^\circ$, dilatancy $\varphi = 0^\circ$, Poisson's ratio $\nu = 0.3$, unit weight $\gamma_{\text{fill}} = 20 \text{ kN/m}^3$ (unless otherwise noted)

$$\frac{E}{P_a} = K_E \left(\frac{\sigma'_3}{P_a} \right)^M$$

and a stress-dependent Young's modulus based on Janbu's equation (Janbu, 1963) viz. where E is Young's modulus, P_a is atmospheric pressure, σ'_3 is the minor effective principal stress, K_E is a material constant (250) and M is a material constant (0.5). Embankment construction was simulated in lifts by incrementally increasing the body forces due to gravity for elements within each lift and in all cases a granular working mat of 0.375 m was placed directly on the foundation soil. The geosynthetic reinforcement was modelled with a linear tensile stiffness, J (kN/m), which was varied, and using a fill-reinforcement interface friction angle of 32° .

In adopting the above parameters for embankment fill, it is assumed that the fill material will approach the critical void ratio and achieve a state of constant volume deformation at failure of the reinforced embankment. As a result, shear resistance of the embankment fill may be underestimated for dense granular materials that exhibit peak shear strength in excess of the constant volume strength. However, given that large deformations occur at failure of reinforced embankments on soft clayey foundations (e.g. Bergado et al., 1994; Rowe et al., 1995), the assumed fill shear strength properties are considered to be adequate and conservative for development of a simplified design approach.

The foundation soils were modelled as having a unit weight $\gamma_{\text{bulk}} = 16.5 \text{ kN/m}^3$ and an undrained shear strength which increased with depth at a rate ρ_c from a value of c_{u0} at the foundation surface. Anisotropy and progressive failure of the foundation soil were not considered. In the present study, the foundation is

assumed to comprise isotropic linear-elastic perfectly plastic material, and consequently, more complex constitutive responses of the foundation have not been assessed. The undrained elastic modulus of the foundation soil, E_u , was assumed to be related to the undrained shear strength, c_u , and the ratio of E_u/c_u was varied between 125 and 500. Initial stresses were generally calculated assuming $K'_0 = 0.7$ and it was found that, although the initial stress state influenced the magnitude and distribution of reinforcement strains at fill thickness below contiguous plasticity, it did not affect the magnitude or distribution of reinforcement strains at failure. The fill thickness at contiguous plasticity is defined by Rowe and Soderman (1985) as the fill thickness where the plastic zones within the foundation soil become continuous resulting in the development of a potential failure plane (this is referred to as primary failure by Bergado et al., 2002).

The finite element model utilized 3-noded linear strain triangles and incorporated 2-noded rigid-perfectly plastic slip elements to allow for slip at the geosynthetic reinforcement-fill interface, clay-fill interface and at the interface between the foundation soil and rigid base. The shear resistance of the clay-fill interface was assumed to be equal to the undrained shear strength of the foundation at the ground surface. The suitability of the finite element meshes were verified by comparing calculated collapse loads with analytical solutions for rigid footing problems. The finite element procedure employed in this paper has been successfully used by Rowe (1982) to study the Pinto Pass embankment and by Rowe and Soderman (1984) to study the Almere test embankment.

4. Factors affecting reinforcement strains at failure

4.1. Embankment failure

Reinforced embankments constructed quickly on soft clay foundations may fail due to excessive displacements before the reinforcement reaches its ultimate tensile strain or performance limit strain. To account for this, Rowe and Soderman (1987) introduced the concept of net embankment height and allowable compatible reinforcement strain.

Fig. 3 shows both the calculated net embankment height and maximum reinforcement strain for an embankment constructed quickly on a soft clayey foundation with $c_{u0} = 3.8$ kPa and $\rho_c = 1.5$ kPa/m. Failure of the reinforced embankment due to excessive subsidence occurs at a fill thickness equal to 2.4 m and the maximum reinforcement strain is 5.2 per cent. There are many geosynthetic materials suitable for reinforcement applications which have a similar stiffness ($J = 600$ kN/m) but with a strain at failure greater than 5.2 per cent. Placement of fill beyond a thickness of 2.4 m for the embankment shown in Fig. 3 will degrade embankment performance without increasing the height of embankment fill above the original ground surface. For this reason, it is important to define the failure thickness of a reinforced embankment as the fill thickness corresponding to the maximum net embankment height. Other limit states for a reinforced embankment

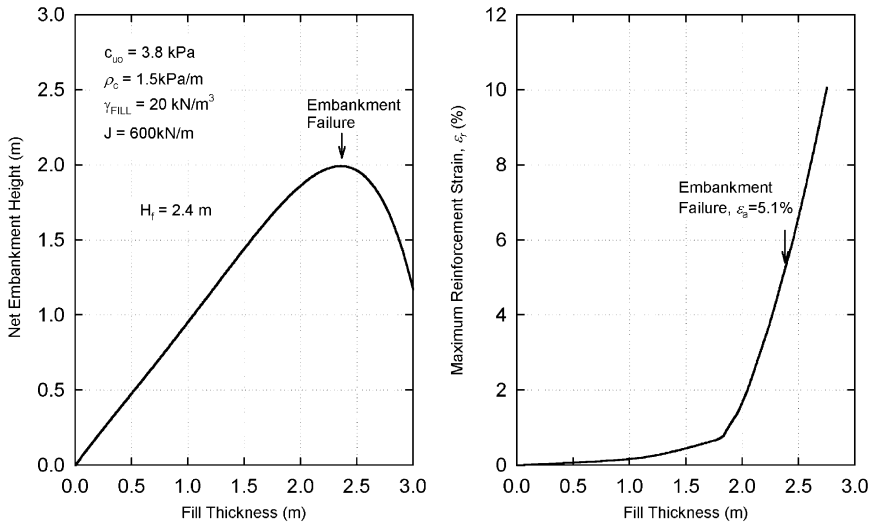


Fig. 3. Maximum net embankment height and allowable compatible reinforcement strain.

include tensile failure of the reinforcement, pullout of the reinforcement or bearing capacity failure of the foundation soil. The most efficient embankment design would involve the simultaneous mobilization of two or more limit states within the embankment (i.e. maximum net embankment height and tensile failure of the reinforcement).

4.2. Effect of reinforcement tensile stiffness

The construction of several embankments to failure was numerically simulated for an embankment with $B = 18 \text{ m}$, $n = 2$ (see Fig. 1) and where the depth to the rigid base was selected so that it had no influence on the kinematics or geometry of the failure mechanism. In general, the depth of the foundation layer, D , was selected on the basis of limit equilibrium calculations and reviewed upon calculation of the velocity field and the resultant failure plane. For the present example, the depth to the rigid base was varied between 2 and 2.5 times the depth of the failure plane. The effect of increasing reinforcement stiffness on embankment response is summarized in Fig. 4 ($c_{u0} = 11.5 \text{ kPa}$ and $\rho_c = 1.5 \text{ kPa/m}$). For reinforcement tensile stiffness below a critical value J_{crit} (see Fig. 4), the reinforcement strain at failure (determined using the maximum net embankment height) was essentially constant at a value called the critical strain, ϵ_0 (8.8% in this case). Over this range of stiffness below J_{crit} ($J < J_{\text{crit}}$), the reinforcement stiffness was found to have only a small influence on the fill thickness at which contiguous plasticity develops in the foundation soil. The weight of fill added after contiguous plasticity has developed in the foundation is supported primarily by the geosynthetic reinforcement. Reinforced embankments

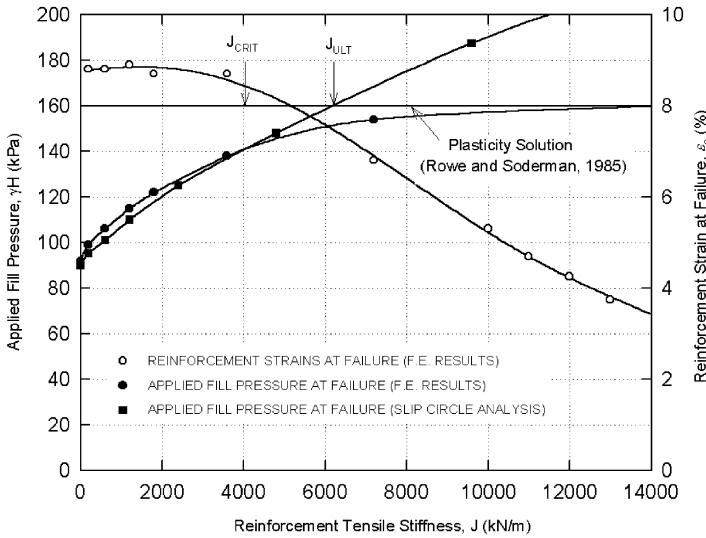


Fig. 4. The influence of reinforcement tensile stiffness on FE embankment behaviour and modified slip circle approximation.

with reinforcement tensile stiffness below J_{crit} will be referred to as “under reinforced” for the remainder of this paper.

The second range of embankment behaviour occurs for reinforcement stiffness above J_{crit} . Here the applied fill pressure approaches the maximum that can be supported by the foundation soil based on bearing capacity (as obtained from plasticity solutions) while the reinforcement force approaches a constant value. The stiffness of the reinforcement over this range begins to influence the kinematics of failure and the fill thickness at which contiguous plasticity is reached within the foundation. The geosynthetic reinforcement forces the failure mechanism to extend deeper into the foundation soil (e.g. Rowe and Mylleville, 1989) and interaction between reinforcement, embankment fill, and foundation soil becomes more complex.

For the purpose of embankment design, the reinforcement strain may be assumed constant at ϵ_0 for reinforcement stiffness below J_{crit} . The results of slip circle calculations assuming a reinforcement force, $T = J \times \epsilon_0$ ($\epsilon_0 = 8.8\%$) for this particular case are also shown in Fig. 4. For the slip circle limit equilibrium calculations, the force was assumed to be constant at ϵ_0 over the length of reinforcement (e.g. Tandjiria et al., 2002) and the reinforcement force was assumed to act in the initial horizontal plane. In Fig. 4, the limit equilibrium calculations are comparable to the finite element results provided that the rigid footing solution is used as an upper bound for the fill pressure at failure. Limit equilibrium calculations utilizing ϵ_0 tend to overestimate the effect of reinforcement for $J > J_{crit}$. Consequently, the correction factor presented in Table 1, α_r , is introduced for embankment design. The correction factor, α_r , is derived from Fig. 4 and represents

Table 1
Reinforcement correction factor, α_r

Reinforcement ratio $(h - H_c)/(H_u - H_c)$	Correction factor, α_r
≤ 0.7	1.0
0.8	1.15
0.9	1.4
1.0	2.0

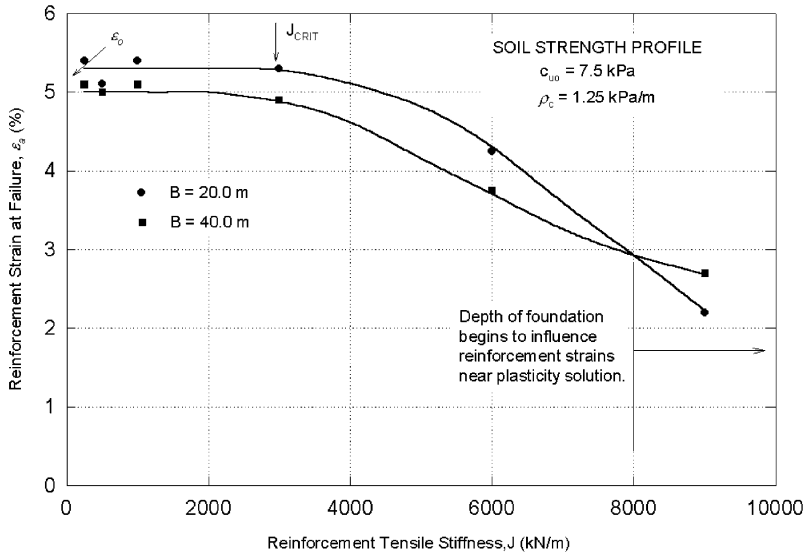


Fig. 5. The effect of embankment crest width on the maximum reinforcement strain at failure.

the ratio of J_{FE} (finite element results) to J_{LE} (limit equilibrium results) for a given applied fill pressure. The use of α_r in design is illustrated in Section 6.

The “under reinforced” range of behaviour ($J < J_{crit}$) will be the focus of the development of a simplified method of analysis and Fig. 2. For $J < J_{crit}$ the allowable compatible strain ϵ_a is equal to the critical strain (i.e. $\epsilon_a = \epsilon_0$) for a particular embankment geometry and soil profile. Fig. 2 summarizes this relationship and the subsequent sections will explain how Fig. 2 was developed.

4.3. Effect of embankment crest width, B

Fig. 5 shows the effects of increasing reinforcement tensile stiffness on reinforcement strain at failure for embankments with crest widths, B , of 20 and 40 m, respectively. The corresponding soil strength parameters are $c_{u0} = 7.5$ kPa and $\rho_c = 1.25$ kPa/m and the foundation depth was selected so that it was sufficiently

large to have no influence on the kinematics of failure in the “under reinforced” range of reinforcement stiffness. Using the same procedure described in Section 4.2, the foundation depth was selected on the basis of limit equilibrium calculations and it varied between 2 and 2.5 times the depth of the failure mechanism. The calculated behaviour indicates that both embankments have a well defined “under reinforced” range and the difference between the maximum reinforcement strains at failure in the “under reinforced” range is of no practical significance. An allowable compatible reinforcement strain, ε_a , of approximately 5% would be suitable for the design of both reinforced embankments.

Referring to Fig. 5, it is apparent that, as the reinforcement becomes very stiff (greater than 8000 kN/m), the calculated reinforcement strain at failure for $B = 40$ m begins to exceed the calculated reinforcement strain at failure for $B = 20$ m. For reinforcement stiffness in excess of J_{crit} , the applied pressure at failure tends towards the rigid footing solution and the D/B ratio begins to influence both the failure kinematics and the resulting reinforcement strains at failure. The effect of the D/B ratio on rigid footing solutions is well known (e.g. Rowe and Soderman, 1987) and will be discussed further in a subsequent section.

It was generally found that for other embankment geometries and soil profiles, the crest width of the embankment had an insignificant impact on the calculated reinforcement strains at failure provided that the foundation depth did not influence the geometry or kinematics of failure. Intuitively, this finding makes sense. Fig. 6 shows the velocity fields at failure for the two embankments considered above in Fig. 5 and for $J = 600$ kN/m. Both the geometry and size of the failure mechanism at failure are essentially the same and crest width does not have a significant impact on embankment behaviour in the “under reinforced” range. It is interesting to note that the embankment crest width has no impact on the collapse height or the geometry of failure mechanism for similar unreinforced embankments with crest width $B = 20$ and 40 m. The negligible effect of embankment crest width on the reinforcement strains at failure is also supported in the literature by Rowe and Soderman (1987) and Rowe and Myllevile (1990) for embankment crest widths of 30 and 18 m, respectively. For the present study, embankment crest width was varied between 10 and 40 m.

4.4. Effects of undrained shear strength, c_{u0}

The influence of undrained shear strength at the foundation surface, c_{u0} , is shown in Fig. 7 for ρ_c equal to 1.5 kPa/m. For c_{u0} less than 11.5 kPa, the behaviour during the “under reinforced” range of behaviour conforms to typical embankment behaviour. Initially the reinforcement strains at failure remain relatively constant at ε_0 . The reinforcement strain at failure in the “under reinforced” range increases as the undrained shear strength at the foundation surface increases from 3.8 to 11.5 kPa. This behaviour reflects the influence of scale on the critical reinforcement strain, ε_0 . As the value of c_{u0} increases, so too does the size of the embankment and the associated failure mechanism. This leads to an increase in the strain in the reinforcement layer.

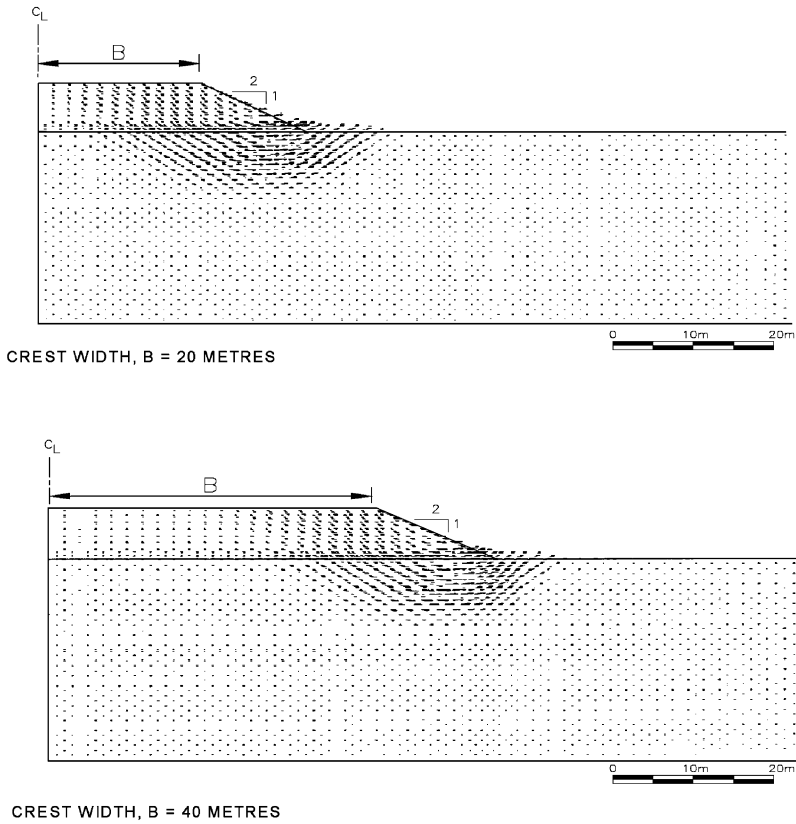


Fig. 6. Comparison of velocity fields at failure for $B = 20$ and 40 m and reinforcement stiffness, $J = 600$ kN/m.

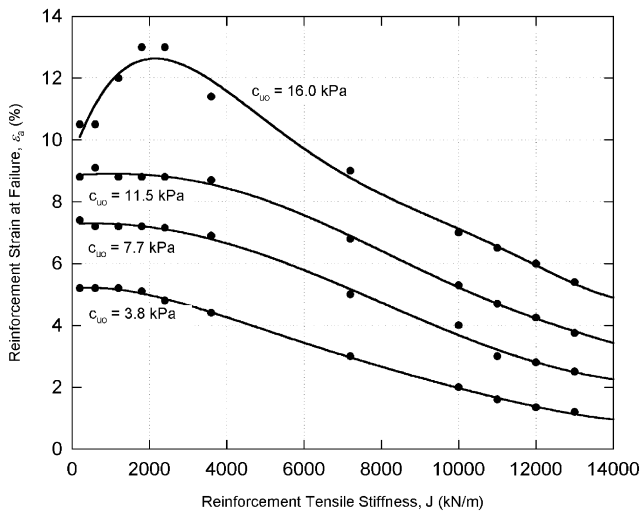


Fig. 7. The effect of c_{u0} on reinforcement strains at failure for $\rho_c = 1.5$ kPa/m.

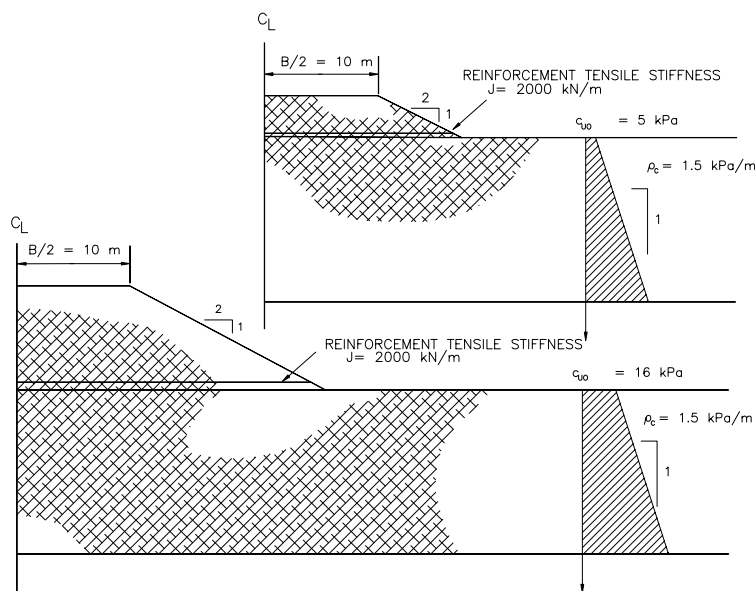


Fig. 8. Zones of plasticity at failure for $c_{u0} = 5$ and 16 kPa.

For c_{u0} greater than 16 kPa, there is no well defined “under reinforced” range of embankment behaviour. As the fill thickness at failure increases, the interaction between the reinforcement, embankment, and foundation becomes more complex. At failure of the reinforced embankment, there are zones of embankment fill that are at a stress state below failure and this has some effect on the calculated reinforcement strains. Fig. 8 shows the zones of plastic soil for the two values of c_{u0} under consideration (i.e. 5 and 16 kPa, $\rho_c = 1.5$ kPa/m and $J = 2000$ kN/m). On the basis of the numerical results presented in Fig. 8, it appears that, at failure for higher embankments, there is potential for arching (Terzaghi et al., 1996) within the embankment fill. This arching produces non-ideal behaviour in the “under reinforced” range.

The absence of a well defined “under reinforced” range of embankment behaviour, however, is of little consequence since the strains are well above what would normally be permitted in typical reinforcement. Also, it is considered conservative to neglect the increase in reinforcement strain above that expected for very little reinforcement. Consequently, in the following sections, the critical reinforcement strain will be limited to that expected for low reinforcement stiffness in the absence of a well defined “under reinforced” range of behaviour.

4.5. Effect of increasing shear strength with depth, ρ_c

Fig. 9 shows the impact of ρ_c on the reinforcement strains at failure for a constant c_{u0} of 10 kPa. Again, the depth to the rigid base was selected so that it had no

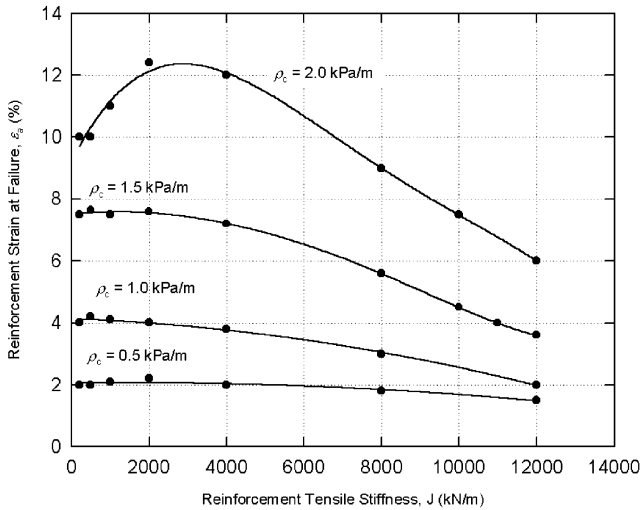


Fig. 9. The effect of ρ_c on the maximum reinforcement strains at failure for $c_{u0} = 10$ kPa.

influence on the kinematics of failure. The maximum reinforcement strain at failure increases as the rate of undrained shear strength with depth increases from 0.5 to 1.5 kPa/m. As ρ_c increases the depth of the failure mechanism that develops within the foundation soil decreases (Hinchberger, 1996). Accordingly, the horizontal component of deformation resulting from plastic flow of the foundation soil increases relative to the vertical component and the resultant reinforcement strains at the maximum net (failure) embankment height increase.

For the case where $\rho_c = 2.0$ kPa/m, there is no well defined “under reinforced” range of embankment behaviour. As discussed earlier, this type of response is due to the increased fill thickness and arching of the embankment fill at failure. In this and similar cases, the critical reinforcement strain ε_0 was limited to that for a small amount of reinforcement or low reinforcement stiffness (e.g. $\varepsilon_0 = 10\%$ in the case of $c_{u0} = 10$ kPa and $\rho_c = 2$ kPa/m).

4.6. Effect of undrained modulus, E_u

Analyses were performed for a number of embankments and for different values of the foundation soil undrained Young’s modulus to strength ratio (E_u/c_u). For a given strength profile it was found that, while there was a difference in deformations at low embankment height, the applied pressure-reinforcement strain curve converged after contiguous plasticity was reached and fill thickness at failure was the same for E_u/c_u ratios of 125 and 500 (Hinchberger, 1996). This occurs because at low fill thickness or applied fill pressure the calculated soil stresses are mainly below failure and the embankment response is governed primarily by Young’s modulus of the foundation soil. However, once contiguous plasticity develops, the equilibrium of the system is controlled by force in the reinforcement and in the soil the plastic

strains dominate elastic strains. This is consistent with the earlier findings of Rowe and Soderman (1987).

5. Design chart

5.1. Reinforcement strains

The results of an extensive series of finite element analyses similar to those already discussed were synthesized to obtain the design curves given in Fig. 2. The curves were based on the critical strain, ε_0 , obtained from finite element analysis in the “under reinforced” range (e.g. see Figs. 5, 7 and 9). As previously noted, in the absence of ideal “under reinforced” behaviour (e.g. Figs. 7 and 9) the reinforcement strain for use in design was limited to the strain calculated for very low reinforcement stiffness.

For reinforcement stiffness, J , less than or equal to J_{crit} , the reinforcement strains at failure were essentially constant (at ε_0) and independent of reinforcement stiffness, J . Thus the allowable compatible reinforcement strain, ε_a , was taken to be equal to the critical strain ($\varepsilon_a = \varepsilon_0$) for $J < J_{\text{crit}}$. As is evident from Figs. 7 and 9, the critical reinforcement strain is dependent on c_{u0} and ρ_c . Rather than using c_{u0} to evaluate reinforcement strains at failure, it was found to be more convenient to represent the effects of c_{u0} in terms of the unreinforced embankment collapse height, H_c . There were several reasons for this. Firstly, the unreinforced embankment collapse height, H_c , must be calculated as the first step in embankment design. Secondly, H_c represents the beginning point for the development of significant reinforcement strains in the “under reinforced” range of embankment behaviour. Also, the unreinforced embankment collapse height, H_c , is directly related to the undrained shear strength of the foundation soil. Finally, the use of H_c enables the design procedure to easily take into account different embankment side slopes and fill unit weight, γ_{fill} , as will be illustrated in the following sections.

5.2. Unit weight of embankment fill, γ_{fill}

Fig. 10 shows calculated fill thickness at failure, $H_f = 3.9$ m, for an embankment constructed with fill having a unit weight of 17.5 kN/m^3 compared to $H_f = 3.3$ m for fill with a unit weight of 20.0 kN/m^3 . The calculated results are based on finite element analysis and the corresponding critical reinforcement strains, ε_0 , are 5.7% ($H_f = 3.9$ m and $\gamma_{\text{fill}} = 17.5 \text{ kN/m}^3$) and 5.0% ($H_f = 3.3$ m and $\gamma_{\text{fill}} = 20 \text{ kN/m}^3$). The corresponding unreinforced embankment collapse heights, H_c , are 3.2 and 2.7 m, respectively. Using Fig. 2 for $H_c = 3.2$ and 2.7 m, the estimated reinforcement strains at failure are 5.4% and 5.1%. For the two cases illustrated in Fig. 10, there is reasonable agreement between strains estimated using Fig. 2 and strains calculated using more elaborate finite element methods. In general, the use of H_c in design allows for consideration of the effect of γ_{fill} on reinforcement strains at failure.

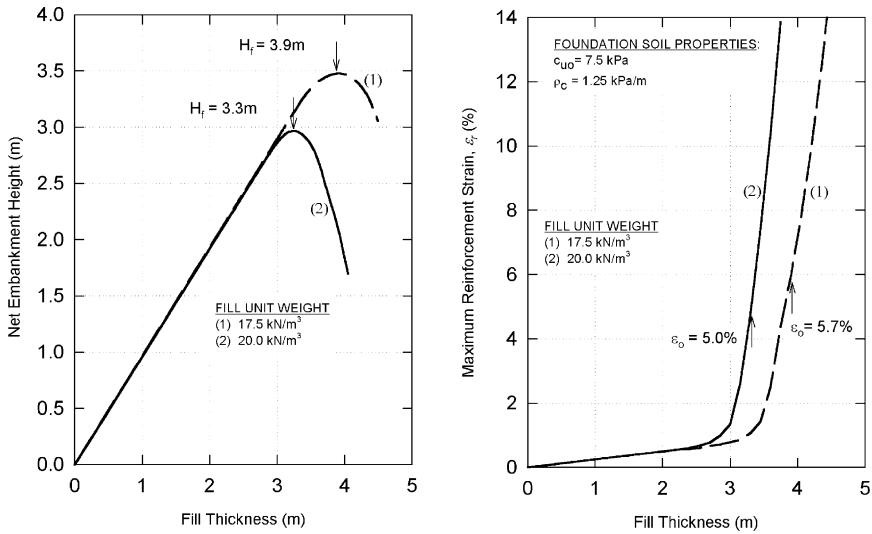


Fig. 10. The effect of fill unit weight, γ_{fill} , on reinforcement strains.

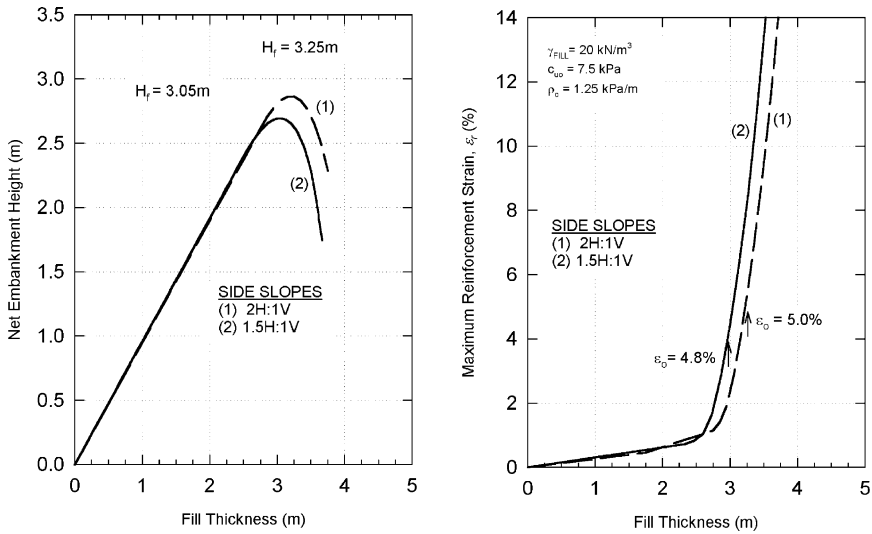


Fig. 11. The effect of embankment side slopes on reinforcement strains.

5.3. Embankment side slopes

Fig. 2 can also be used to account for the impact of embankment side slopes on ϵ_a . To illustrate, Fig. 11 shows the calculated net embankment height versus fill thickness for embankments with 2H:1V side slopes and 1.5H:1V side slopes. The soil strength properties adopted for the analysis were $c_{u0} = 7.5\text{ kPa}$, $\rho_c = 1.25\text{ kPa/m}$. Based on the finite element results presented in Fig. 11, the calculated reinforcement

strain at failure, ε_0 , is 5.0% and 4.8% for side slopes of 2H:1V and 1.5H:1V, respectively. Using equilibrium methods and Fig. 2, the estimated critical reinforcement strain, ε_0 , is 5.1% ($H_c = 2.74$ m) and 4.8% ($H_c = 2.5$ m) for side slopes of 2H:1V and 1.5H:1V. Overall, there is a reduction in critical reinforcement strain resulting from a change in the kinematics of the failure mechanism. Steeper side slopes (1.5H:1V) reduce the lateral deformations at failure (kinematics) and hence reduce the reinforcement strains at failure. This is consistent with the findings of Rowe and Soderman (1985) for embankments constructed on homogeneous foundation soils. The foregoing serves to illustrate that the change in critical strain, ε_0 , due to changing side slope geometry can be approximately accounted for using the failure height of the unreinforced embankment, H_c , and Fig. 2.

5.4. Depth of foundation soil layer, D

The design curves presented in Fig. 2 were derived for cases where the depth of the foundation soil layer did not influence the kinematics at failure in the “under reinforced” range of behaviour and hence the reinforcement strains at failure. Rowe and Soderman (1987) found that reducing the depth to the rigid boundary, D , increased both the failure height and the reinforcement strains at failure for embankments constructed on soft homogeneous soil deposits. The present study has also found this to be the case for reinforced embankments constructed on soft clayey foundations having increasing strength with depth, ρ_c . Therefore, the reinforcement strains presented in Fig. 2 are minimum values. If the depth of the rigid base is sufficiently small to restrict the depth of the failure mechanism, lateral deformations will increase and the resultant reinforcement strain at failure will increase; under these circumstances the values proposed in Fig. 2 are conservative.

To illustrate the point noted above, Fig. 12 shows reinforcement strains at failure versus reinforcement stiffness for foundation depths of 4, 6 and 20 m, respectively. The critical reinforcement strain, ε_0 , is about 3% for D equal to 6 and 20 m. For $D = 4$ m, however, the depth of the rigid boundary is sufficiently small to influence the kinematics at failure and produce non-ideal embankment behaviour in the “under reinforced” range. The results show that neglecting the presence of the rigid base yields estimated reinforcement strains that are less than those observed for shallow soil deposits. For the purpose of design, neglecting the impact of foundation depth on the critical strain and using values given in Fig. 2 is considered to be adequate.

6. Worked examples

6.1. Example 1

A 3.2 m thick embankment with 2H:1V side slopes and 18 m crest width is to be constructed on a 20 m thick deposit of soft clay. The clay deposit has an undrained shear strength defined by $c_{u0} = 10$ kPa and $\rho_c = 1.5$ kPa/m. The unit weight of the

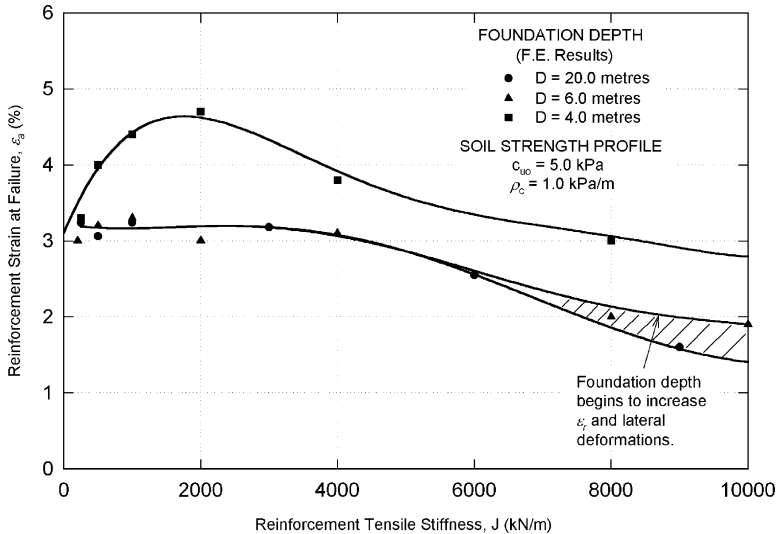


Fig. 12. The effects of foundation depth on the maximum reinforcement strains at collapse.

proposed fill is approximately 20 kN/m^3 and the factored friction angle, ϕ' , was taken to be 30° . The partial factor adopted for granular fill was 0.8 in accordance with the Ontario Highway Bridge Design Code (Ministry of Transportation of Ontario, 1983). The corresponding unfactored friction angle is $\phi' = 36^\circ$. The design proceeds as follows:

(i) *Obtain factored foundation strength parameters.* The first step in design is to factor the foundation soil strength properties using appropriate partial factors. Here, $PF = 1/1.3 = 0.77$ and hence $c_{u0}^* = 7.7 \text{ kPa}$, $\rho_c^* = 1.2 \text{ kPa/m}$.

(ii) *Unreinforced collapse height, H_c .* Using slip circle analysis, the collapse height of an unreinforced embankment constructed on the factored soil profile ($c_{u0}^* = 7.7 \text{ kPa}$, $\rho_c^* = 1.2 \text{ kPa/m}$) was found to be approximately $H_c = 2.7 \text{ m}$. This is less than the required fill thickness of 3.2 m and indicates that reinforcement is required.

(iii) *Bearing capacity limits for perfectly reinforced embankment.* Having established that reinforcement is required to provide the required factor of safety (at $h = 3.2 \text{ m}$), it is necessary to estimate the maximum possible increase in fill thickness that may be attained by heavily reinforcing the embankment. In the manner proposed by Rowe and Soderman (1987) and illustrated by Rowe and Mylleville (1993) and Leroueil and Rowe (2001), the embankment was idealized as a rigid footing with surcharge. The collapse height was estimated to be approximately $H_u = 4.65 \text{ m}$ for the factored soil strength parameters ($c_{u0}^* = 7.7 \text{ kPa}$, $\rho_c^* = 1.2 \text{ kPa/m}$). Since H_u exceeds the design fill thickness of 3.2 m, it indicates that the required embankment height may be achieved with reinforcement.

(iv) *Allowable reinforcement strain.* For an unreinforced collapse height $H_u = 2.7 \text{ m}$ and increasing shear strength with depth, $\rho_c^* = 1.2 \text{ kPa/m}$, the allowable

compatible reinforcement strain is approximately $\varepsilon_a = 5$ per cent (Fig. 2). Since the reinforcement strain at failure was estimated based on the factored soil strength profile there is no need to factor this value further.

(v) *Stability of reinforced embankment.* Using limit equilibrium methods REAP3.0 (Rowe and Mylleville, 1987), the required reinforcement force at a fill thickness of 3.2 m was calculated to be $T_r = 24$ kN/m. This reinforcement force along with the allowable reinforcement strain ε_a may be used to specify a minimum required reinforcement stiffness as follows:

Estimate the correction factor, α_r

$$\frac{(H - H_c)}{(H_u - H_c)} = \frac{(3.2 \text{ m} - 2.7 \text{ m})}{(4.65 \text{ m} - 2.7 \text{ m})} = 0.26$$

$\alpha_r = 1.0$ (from Table 1).

$J_{\min} = \alpha_r T_r / \varepsilon_a = 1.0 \times 24.0 \text{ kN/m} / 0.05 = 480 \text{ kN/m}$ (over a strain range of 0–5%).

A geosynthetic product which meets the following minimum requirements can now be selected: (i) suitable for reinforcement applications, (ii) a minimum secant stiffness of 480 kN/m over a strain range of 0–5% and (iii) a performance limit strain greater than or equal to 5 per cent. It should be noted that rather than specifying a single layer of reinforcement with $J = 480$ kN/m, an alternative would be to use two layers of closely spaced reinforcement (e.g. 300 mm) with $J = 480/2 \approx 250$ kN/m (see Rowe and Mylleville, 1990).

The final step in the design is to check other failure mechanisms such as the pullout resistance of the geosynthetic reinforcement. This is straightforward and will not be illustrated here.

6.2. Example 2

The second design example illustrates the limiting case of what can be achieved with reinforcement. Utilizing the soil strength properties and geometry from Example 1, it is assumed that an embankment height of 4.65 m is required. Steps (i) through (iv) are identical and accordingly the design will begin at step (v).

(v) *Stability of reinforced embankment:* Using slip circle analysis, the reinforcement force required to achieve a fill thickness of 4.65 m (i.e. equal to the value possible based on bearing capacity) is $T_r = 210$ kN/m. Utilizing the allowable reinforcement strain at collapse, $\varepsilon_a = 0.05$, the minimum reinforcement stiffness required to obtain a perfectly reinforced embankment is obtained as follows:

$$\frac{(H - H_c)}{(H_u - H_c)} = \frac{(4.65 \text{ m} - 2.7 \text{ m})}{(4.65 \text{ m} - 2.7 \text{ m})} = 1.0$$

$\alpha_r = 2.0$ (from Table 1).

$J_{\min} = \alpha_r T_r / \varepsilon_a = 2.0 \times 210 \text{ kN/m} / 0.05 = 8400 \text{ kN/m}$ (over a strain range of 0–5%).

To complete the current design, a geosynthetic product must be selected with a minimum reinforcement tensile stiffness, J , of approximately 8400 kN/m, a performance limit strain in excess of 5 per cent with adequate pull-out resistance.

In this case, multiple reinforcement layers are likely required to achieve the desired fill thickness.

7. Case history—Sackville N.B. test embankment

A fully instrumented geosynthetic reinforced test embankment was constructed to failure on a soft silty clay deposit near Sackville New Brunswick, Canada. Detailed measurements of pore pressures, geotextile strains, and displacements were recorded during construction. Rowe et al. (1995) provide a detailed description of the embankment construction and performance in the literature and only essential details of the case history will be summarized here.

Fig. 13 shows the test embankment geometry and soil strength profile obtained from in situ cone penetration and field vane test (see Rowe et al., 1995). Tables 2 and 3 contain a summary of the embankment fill and geotextile properties, respectively.

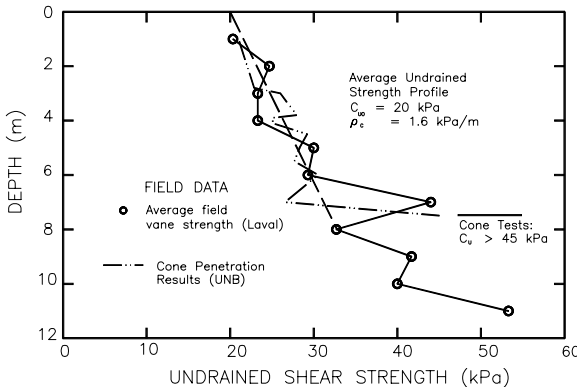
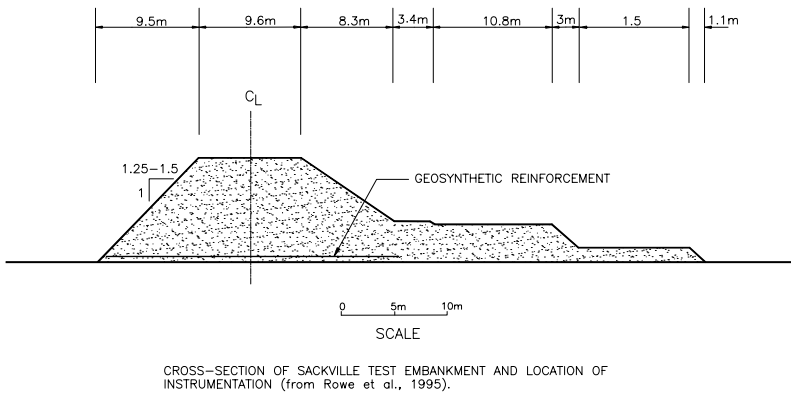


Fig. 13. Soil strength profile and embankment geometry of the Sackville test embankment (modified from Rowe et al., 1995).

Table 2
Embankment fill shear strength parameters (Gnanendran, 1993)

Material property	Peak envelope	Residual envelope
c'	17.5 kPa	10 kPa
ϕ'	38°	34°

Table 3
Geotextile properties (Gnanendran, 1993)

Material property	Value
Unit weight	631 g/m ²
Modulus, J	1920 kN/m
$\phi'_{\text{interface}}$	42°
Failure strain, ε_f	13%

The soil strength profile obtained from in situ tests indicates that the undrained shear strength at the foundation surface, c_{u0} is approximately 20 kPa. The gradient of undrained shear strength with depth, ρ_c , is 1.6 kPa/m (see Fig. 13). Below a depth of about 8 m, the increase in undrained shear strength with depth, ρ_c , increases to approximately 2.5 kPa/m. Based on the depth of the critical failure surface obtained using slip circle analysis and the failure surface observed during construction by Rowe et al. (1995), $\rho_c = 1.6$ kPa/m was selected for use with Fig. 2.

Neglecting the cohesive strength of the embankment fill and adopting a friction angle $\phi' = 38^\circ$, and side slopes of 1H: 1V, the failure height of an unreinforced embankment, H_c , constructed on the Sackville foundation soil was calculated ($H_c = 6.7$ m). Referring to Fig. 2, the critical reinforcement strain corresponding to the maximum net embankment height is approximately 10%. Table 3 indicates that the reinforcement reaches its ultimate tensile strength at an axial strain of approximately 13.0%. Consequently, the predicted reinforcement strain of 10% (Fig. 2) is approaching the ultimate tensile strain of the reinforcement used for the Sackville test embankment. On the basis of the proposed method for estimating reinforcement strains, there is a strong probability that the embankment will reach the maximum net embankment height (failure) at approximately the same time that the reinforcement reaches its failure strain.

Fig. 14 shows the net embankment height versus fill thickness curve for the Sackville test embankment. Due to the time-dependent behaviour of the foundation soil, both upper and lower net embankment height versus fill thickness curves are inferred from the field data. In general, the Sackville test embankment reached its maximum net embankment height at a fill thickness of approximately 8.2 m, supported by both upper and lower bound net embankment height versus fill thickness curves in Fig. 14. The maximum measured reinforcement strains during construction of the Sackville test embankment are also shown in Fig. 14 (Rowe and Gnanendran, 1994). As the fill was advanced from a thickness of 5.7 m to a thickness of 8.2 m, the maximum reinforcement strain increased from 5.4% to 8.6%

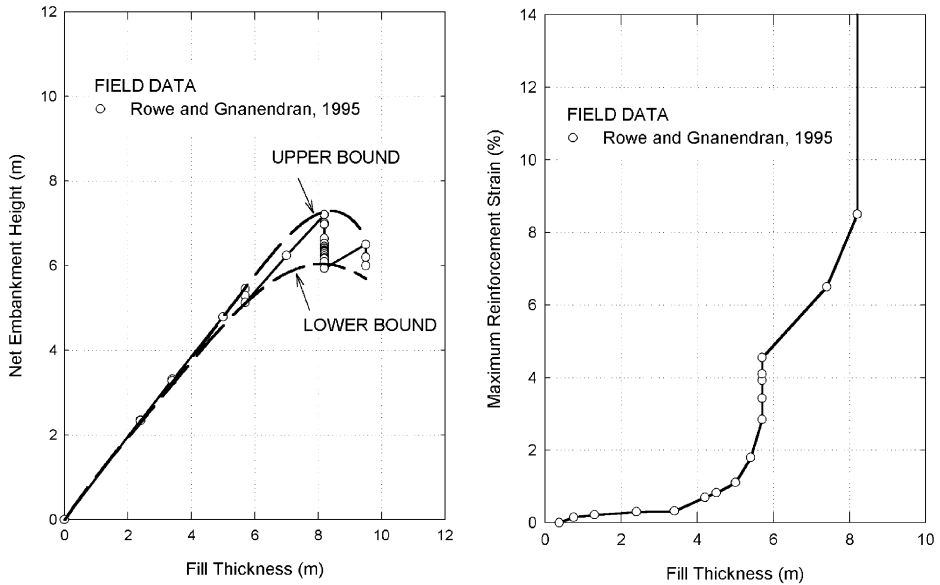


Fig. 14. Maximum reinforcement strains versus fill thickness for the Sackville test embankment.

(Rowe and Gnanendran, 1994). At a fill thickness of 8.2 m, the embankment continued to deform under conditions of approximately constant effective stress (see Rowe et al., 1995; Rowe and Hinchberger, 1998). Rowe et al. (1995) described the failure of the Sackville test embankment as a viscous type of failure and Rowe and Hinchberger (1998) demonstrated that the deformations that occurred during construction stoppages could be modelled using an elasto-viscoplastic constitutive model. The embankment failed while the fill thickness was maintained at 8.2 m and the reinforcement strain at failure was estimated to be between 8.6% and 13.0% (allowing for uncertainties in measurement at a time when there were large deformations occurring).

The reinforcement strain at failure predicted using Fig. 2 is 10%, which lies within the upper and lower bounds inferred from the field performance. The measured performance of the Sackville test embankment suggests that in this case both the reinforcement and the test embankment failed simultaneously. Thus, despite uncertainties associated with the time-dependent nature of the Sackville test embankment failure, the behaviour of the test embankment provides some justification for the proposed design curves in Fig. 2.

8. Summary and conclusions

A method for calculating the allowable reinforcement strains for embankments constructed on soft clayey foundations having increasing undrained shear strength

with depth has been presented. The method was tested against the observed performance of the Sackville, N.B. test embankment case history. Overall, factors such as the undrained shear strength profile (in terms of c_{u0} and ρ_c) strongly influenced the reinforcement strains at failure. It was generally found that the behaviour of reinforced embankments on soft clayey foundations is dominated by plastic flow within the foundation and the resultant kinematics of failure. Elastic properties of both the foundation and embankment material did not have a significant impact on calculated reinforcement strains at failure. It is recognized, however, that a relatively narrow range of fill properties were investigated here and that further research into the influence of fill properties on reinforcement strains is warranted.

The focus of this paper was on failure of reinforced embankments due to excessive displacement. It is noted that modes of failure such as pullout of the reinforcement, and sliding along the foundation-fill interface did not govern failure in the finite element analyses utilized in developing the simplified procedure. As noted in Section 2, these other potential failure modes must be assessed during the design of reinforced embankments on soft clayey foundations.

Overall, the method of analysis proposed here is simplified and approximately takes into account the effects of embankment side slopes and fill unit weight on the reinforcement strains at failure. Combined with simplified methods of analysis (e.g. slip circle) the allowable reinforcement strains can be used to select suitable reinforcement. Finally, two examples were used to illustrate the selection of reinforcement for embankments on soft clayey foundation soil with increasing strength with depth. As with any geotechnical design, engineering judgment is required in assessing the applicability of this, or any other, design method for a given application.

Acknowledgements

The research reported in this paper was funded by a research grant from the Natural Sciences and Engineering Research Council of Canada.

References

- Bergado, D.T., Long, P.V., Lee, C.H., Loke, K.H., Werner, G., 1994. Performance of reinforced embankment on soft Bangkok clay with high-strength geotextile reinforcement. *Geotextiles and Geomembranes* 13, 403–420.
- Bergado, D.T., Long, P.V., Murthy, B.R.S., 2002. A case study of geotextile-reinforced embankment on soft ground. *Geotextiles and Geomembranes* 20, 343–365.
- Bonaparte, R., Christopher, B.R., 1987. Design and construction of reinforced embankments over weak foundations. *Transportation and Research Record*, No. 1153, pp. 26–39.
- den Hoedt, G., 1986. Creep and relaxation of geotextile fabrics. *Geotextiles and Geomembranes* 4 (2), 83–92.

- Fowler, J., Koerner, R.M., 1987. Stabilization of very soft soils using geosynthetics, Proceedings Geosynthetics '87, New Orleans, pp. 289–300.
- Gnanendran, C.T., 1993. Behaviour of geotextile reinforced embankments on soft soils. Ph.D. Thesis. Faculty of Graduate Studies. The University of Western Ontario, London, ON, Canada.
- Hinchberger, S.D., 1996. The behaviour of reinforced and unreinforced embankments on rate sensitive clayey foundations. Ph.D. Thesis, University of Western Ontario.
- Hird, C.C., Kwok, C.M., 1989. Finite element studies of interface behaviour in reinforced embankments on soft ground. *Computers and Geotechnics* 8 (2), 111–131.
- Humphrey, D.N., Holtz, R.D., 1989. Effect of surface crust on reinforced embankments. Proceedings of Geosynthetics '89 Conference, San Diego, USA, pp. 136–147.
- Janbu, N., 1963. Soil compressibility as determined by oedometer and triaxial tests. Proceedings of the European Conference on Soil Mechanics and Foundation Engineering, Vol. 1, Wiesbaden, Germany, pp. 19–25.
- Jewel, R.A., 1982. A limit equilibrium design method for reinforced embankments on soft foundations. Proceedings of Second International Conference on Geotextiles, Vol. 2, Las Vegas, Nevada, USA, pp. 671–676.
- Jewel, R.A., 1988. The mechanics of reinforced embankment on soft soils. *Geotextiles and Geomembranes* 7, 237–274.
- Leroueil, S., Rowe, R.K., 2001. "Embankments over Soft Soil and Peat," Chapter 16 of *Geotechnical and Geoenvironmental Engineering Handbook*. Kluwer Academic Publishing, Norwell, USA, pp. 463–499.
- McGown, A., Yogarajah, I., Andrawes, K.Z., Saad, M.A., 1995. Strain behaviour of polymetric geogrids subject to sustained and repeated loading in air and in soil. *Geosynthetics International* 2 (1), 341–355.
- Michalowski, R.L., 1992. Bearing capacity of nonhomogeneous cohesive soils under embankments. *Journal of Geotechnical Engineering Division, ASCE* 118 (9), 1098–1118.
- Milligan, V., La Rochelle, P., 1984. Design methods for embankments over weak soils. Symposium on Polymer Grid Reinforcement in Civil Engineering, Institute of Civil Engineers, Paper No. 34, London, England, pp. 95–102.
- Ministry of Transportation of Ontario, 1983. Ontario highway bridge design code (and Commentary). Highway Engineering Division, Ministry of Transportation of Ontario, Toronto.
- Palmeira, E.M., Pereira, J.H.F., da Silva, A.R.L., 1998. Backanalyses of geosynthetic reinforced embankments on soft soils. *Geotextiles and Geomembranes* 16, 273–292.
- Rowe, R.K., 1982. The analysis of an embankment constructed on a geotextile. Proceedings of Second International Conference on Geotextiles, Vol. 2, Las Vegas, Nevada, USA, pp. 677–682.
- Rowe, R.K., 1984. Reinforced embankment: analysis and design. *Journal of Geotechnical Engineering Division, ASCE* 110 (2), 231–247.
- Rowe, R.K., Gnanendran, C.T., 1994. Geotextile strain in a full scale reinforced test embankment. *Geotextiles and Geomembranes* 13, 781–806.
- Rowe, R.K., Gnanendran, C.T., Landva, A.O., Valsangkar, A.J., 1995. Construction and performance of a full-scale geotextile reinforced test embankment, Sackville, New Brunswick. *Canadian Geotechnical Journal* 32, 512–534.
- Rowe, R.K., Hinchberger, S.D., 1998. The significance of rate effects in modelling the Sackville test embankment. *Canadian Geotechnical Journal* 35, 500–516.
- Rowe, R.K., Mylleville, B.L.J., 1989. Consideration of strain in the design of reinforced embankments. Proceedings of Geosynthetics '89, San Diego, USA, pp. 124–135.
- Rowe, R.K., Mylleville, B.L.J., 1990. Implications of adopting an allowable geosynthetic strain in estimating stability. Proceedings of the Fourth International Conference on Geotextiles, Geomembranes and Related Products, The Hague, pp. 131–136.
- Rowe, R.K., Mylleville, B.L.B., 1993. The stability of embankments reinforced with steel. *Canadian Geotechnical Journal* 30, 768–780.
- Rowe, R.K., Soderman, K.L., 1984. Comparison of predicted and observed behaviour of two test embankments. *Geotextiles and Geomembranes* 1, 143–160.

- Rowe, R.K., Soderman, K.L., 1985. An approximate method for estimating the stability of geotextile-reinforced embankments. *Canadian Geotechnical Journal* 22 (3), 392–398.
- Rowe, R.K., Soderman, K.L., 1987. Reinforcement of embankments on soils whose strength increases with depth. *Proceedings of Geosynthetics '87*, New Orleans, pp. 266–277.
- Tandjiria, V., Low, B.K., The, C.I., 2002. Effect of reinforcement force distribution on stability of embankments. *Geotextiles and Geomembranes* 20, 423–443.
- Terzaghi, K., Peck, R.B., Mesri, G., 1996. *Article 38 of Soil Mechanics in Engineering Practice*. Wiley, New York, NY, pp. 289–290.